Neuron
Article

M1 Muscarinic Receptors Boost Synaptic Potentials and Calcium Influx in Dendritic Spines by Inhibiting Postsynaptic SK Channels

Andrew J. Giessel[1] and Bernardo L. Sabatini[1,*]
[1]Howard Hughes Medical Institute, Department of Neurobiology, Harvard Medical School, Boston, MA 02115, USA
*Correspondence: bernardo_sabatini@hms.harvard.edu
DOI 10.1016/j.neuron.2010.09.004

SUMMARY

Acetylcholine release and activation of muscarinic cholinergic receptors (mAChRs) enhance synaptic plasticity in vitro and cognition and memory in vivo. Within the hippocampus, mAChRs promote NMDA-type glutamate receptor-dependent forms of long-term potentiation. Here, we use calcium (Ca) imaging combined with two-photon laser glutamate uncaging at apical spines of CA1 pyramidal neurons to examine postsynaptic mechanisms of muscarinic modulation of glutamatergic transmission. Uncaging-evoked excitatory postsynaptic potentials and Ca transients are increased by muscarinic stimulation; however, this is not due to direct modulation of glutamate receptors. Instead, mAChRs modulate a negative feedback loop in spines that normally suppresses synaptic signals. mAChR activation reduces the Ca sensitivity of small conductance Ca-activated potassium (SK) channels that are found in the spine, resulting in increased synaptic potentials and Ca transients. These effects are mediated by M1-type muscarinic receptors and occur in a casein kinase-2-dependent manner. Thus, muscarinic modulation regulates synaptic transmission by tuning the activity of nonglutamatergic postsynaptic ion channels.

INTRODUCTION

Cholinergic fibers from the medial septum and basal forebrain project widely throughout the neocortex and hippocampus (Dutar et al., 1995; Woolf, 1991). Release of acetylcholine (ACh) and activation of muscarinic G protein-coupled acetylcholine receptors (mAChRs) promote vigilance and facilitate learning and memory in a variety of behavioral paradigms (Dawson and Iversen, 1993; Deutsch, 1971; Drachman, 1977; Everitt and Robbins, 1997; Kitajima et al., 1992; Stackman et al., 2002). Furthermore, modulation of cholinergic systems remains one of the few symptomatic treatments for Alzheimer's disease (Mesulam, 2004). Thus, in humans and experimental animals, ACh release and mAChR signaling promote acquisition of new behaviors and facilitate learning in a variety of contexts.

Multiple studies have demonstrated that ACh release and mAChR activation enhance glutamatergic synaptic responses in the central nervous system (Dutar and Nicoll, 1988; Madison et al., 1987; Marino et al., 1998; Markram and Segal, 1990a). In the hippocampus, mAChR agonists promote the induction of NMDAR-dependent long-term potentiation (LTP) at synapses between CA3 and CA1 pyramidal neurons (Fernández de Sevilla et al., 2008; Markram and Segal, 1990b). These actions are mediated by postsynaptically expressed M1-type mAChRs that couple to $G_{\alpha q}$ to activate phospholiapse C (PLC) and mobilize Ca from intracellular stores (Shinoe et al., 2005). Additionally, activation of M2/4 mAChRs on presynaptic boutons may reduce vesicular release probability (Levey et al., 1995; Rouse et al., 1999, 2000). Given the role of the hippocampus in many forms of learning, facilitation of LTP at this synapse may explain many of the behavioral effects of mAChR agonists. Nevertheless, the mechanisms by which ACh enhances synaptic plasticity are unknown.

Glutamatergic synaptic potentials and associated dendritic Ca transients are regulated by a variety of nonglutamate receptor ion channels including voltage-gated Ca, Na, and K channels, as well as SK-type Ca-activated K channels (Andrásfalvy et al., 2008; Bloodgood et al., 2009; Bloodgood and Sabatini, 2007; Faber et al., 2005; Magee, 1999; Magee and Cook, 2000). Many of these ion channels are regulated by mAChRs and other G protein-coupled receptors (GPCRs) (Faber et al., 2008; Maingret et al., 2008; Martina et al., 2007; Ramanathan et al., 2008; Tai et al., 2006), and blockade of these channels alters the properties and plasticity of synapses as well as behavioral learning (Borroni et al., 2000; Hammond et al., 2006; Lin et al., 2008). For example, at CA3 to CA1 synapses, blockade of SK channels boosts the amplitude of synaptic potentials and spine Ca transients and facilitates LTP induction (Bloodgood et al., 2009; Bloodgood and Sabatini, 2007; Ngo-Anh et al., 2005; Stackman et al., 2002). Furthermore, in vivo administration of SK antagonists enhances the acquisition of hippocampal-dependent behaviors (Hammond et al., 2006; Lin et al., 2008). However, the importance of these nonglutamatergic ion channels in regulating synaptic transmission may be underestimated because their opening is often prevented in voltage-clamp studies of synaptic transmission. Conversely, changes in glutamate receptor opening that are inferred from current-clamp and field recordings of synaptic responses or from studies of responses to iontophoretic application of glutamate may be confounded by changes in opening of voltage- or Ca-gated channels. Thus, many of the effects of mAChRs on hippocampal synaptic transmission, plasticity, and hippocampal-dependent

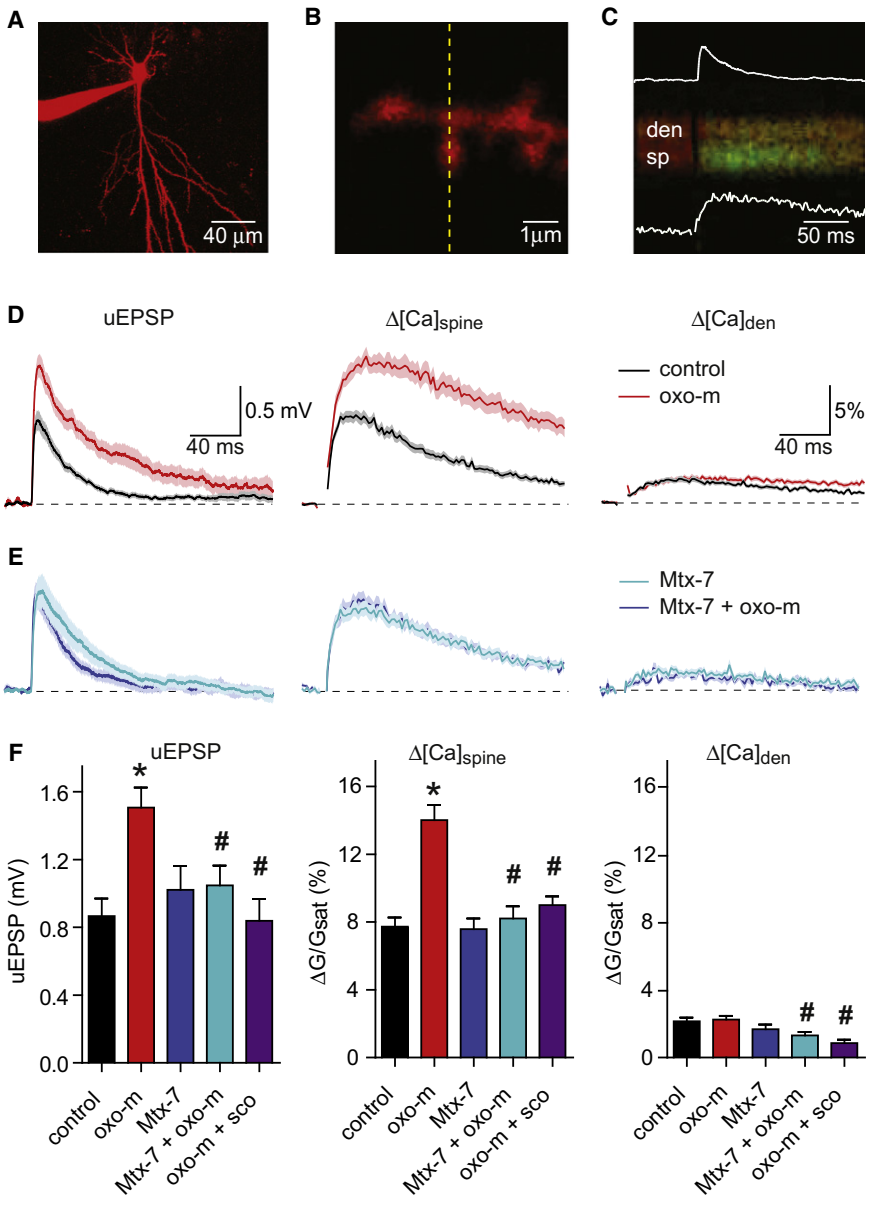

Figure 1. Synaptic Potentials and Ca Transients Evoked at Individual Dendritic Spines of CA1 Pyramidal Neurons Are Enhanced by Activation of mAChRs

(A) Image of a CA1 hippocampal pyramidal neuron formed from the red fluorescence of Alexa Fluor 594.

(B) High-magnification image of a spiny dendrite.

(C) Example of fluorescence collected during line scans, as indicated by the dashed line in (B), that intersect the spine head (sp) and neighboring dendrite (den) during uncaging of glutamate near the spine head. The increase in green fluorescence indicates an increase in intracellular [Ca]. The inset white traces show the simultaneously recorded uEPSP (top, amplitude 0.9 mV) and the quantification of the green fluorescence in the spine head (bottom, amplitude 10.8% $\Delta G/G_{sat}$).

(D) uEPSPs (left) and Ca-dependent changes in fluorescence measured in the spine head (middle) and neighboring dendrite (right) evoked by uncaging glutamate in control conditions (black) and in the presence of oxo-m (red). In this and all subsequent figures, data are shown as the mean (line) ± SEM (shaded region).

(E) uEPSPs (left) and Ca-dependent changes in fluorescence measured in the spine head (middle) and neighboring dendrite (right) evoked by uncaging glutamate in the presence of Mtx-7 (dark blue) and in the additional presence of oxo-m (light blue).

(F) Summary of amplitudes of uEPSPs (left), $\Delta[Ca]_{spine}$ (middle), and $\Delta[Ca]_{den}$ (right) measured in control conditions (black), in the presence of oxo-m (red), M1 receptor antagonist Mtx-7 (blue), Mtx-7 and oxo-m (light blue), and scopolamine (sco) and oxo-m (purple). (*) indicates a significant difference from control ($p < 0.05$), (#), a significant difference from oxo-m alone ($p < 0.05$).

behaviors may be explained by modulation of Ca- or voltage-gated ion channels in the spine.

Here, we examine the effects of mAChRs on postsynaptic glutamatergic responses in CA1 pyramidal neurons of mouse hippocampus. We use two-photon laser uncaging (2PLU) of glutamate to stimulate individual, visualized postsynaptic terminals and two-photon laser scanning microscopy (2PLSM) with simultaneous whole-cell recordings to monitor synaptic Ca transients and evoked potentials. We find that activation of mAChRs enhances the magnitude of synaptic potentials and Ca transients generated by activation of a single postsynaptic terminal. However, mAChRs do not regulate the intrinsic properties of AMPA- and NMDA-type glutamate receptors (AMPARs and NMDARs, respectively). Instead, the enhancement of synaptic signals by mAChRs results from modulation of SK channels present in dendritic spines. mAChR-dependent inhibition of SK is due to a reduction of the Ca sensitivity of the channels and occurs in a casein kinase-2 (CK2)-dependent manner. In summary, our studies elucidate the effects of mAChRs on postsynaptic signaling at CA3 to CA1 synapses and reveal a mechanism by which their activation likely promotes plasticity induction.

RESULTS

In order to determine the postsynaptic effects of mAChR activation on glutamatergic synapses, we examined responses evoked by 2PLU of glutamate onto apical spines of CA1 pyramidal neurons (Figure 1). Whole-cell current-clamp recordings were obtained from neurons in acute slices of mouse hippocampus (postnatal day 15–18) using a K-based intracellular solution containing the red-fluorescing Ca-insensitive fluorophore Alexa Fluor 594 (10 μM) and the green-fluorescing Ca-sensitive fluorophore Fluo-5F (300 μM) (Carter and Sabatini, 2004).

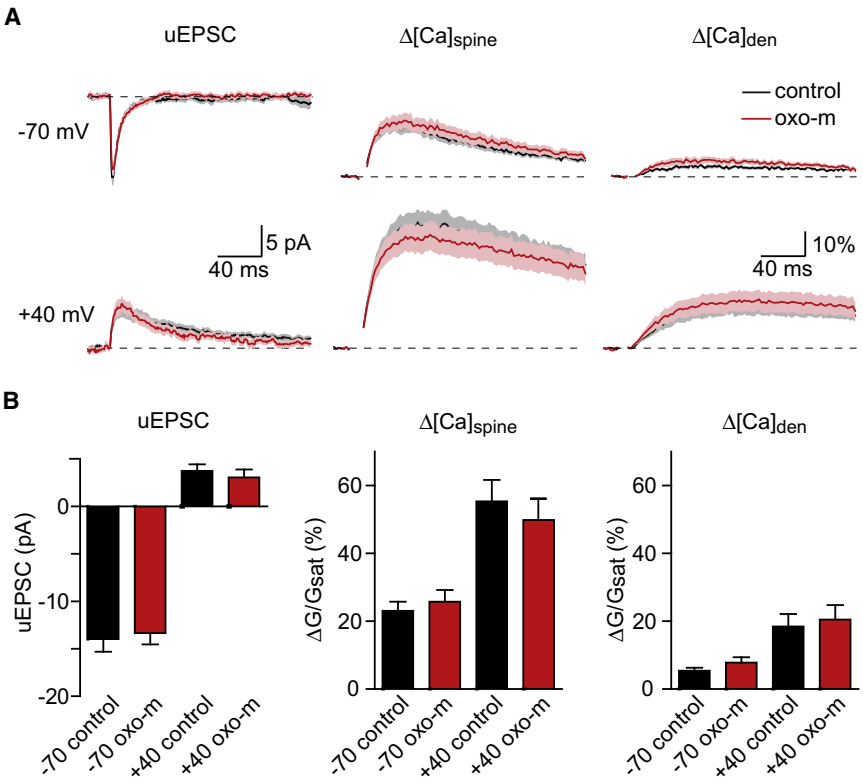

Figure 2. Current through AMPARs and NMDARs and the Ca Permeability of NMDARs Are Unaffected by Activation of mAChRs

(A) uEPSCs (left), $\Delta[Ca]_{spine}$ (middle), and $\Delta[Ca]_{den}$ (right) evoked by stimulating individual spines while holding the cell at −70 mV (top) and +40 mV (bottom). Black and red traces are in control conditions and in the presence of oxo-m, respectively.

(B) Summary of amplitudes of uEPSCs (left), $\Delta[Ca]_{spine}$ (middle), and $\Delta[Ca]_{den}$ (right) measured in the conditions described above.

2PLSM was used to visualize cellular and dendritic morphology and to monitor intracellular Ca transients (Figures 1A–1C). Individual dendritic spines were stimulated by photoreleasing glutamate using 500 μs pulses of 725 nm laser light directed at a spot near the spine head (see Experimental Procedures). This resulted in an uncaging-evoked postsynaptic potential (uEPSP) detectable at the soma as well as increases in green fluorescence ($\Delta G/G_{sat}$, see Experimental Procedures) in the spine head and neighboring dendrite, indicative of elevated [Ca] in each compartment ($\Delta[Ca]_{spine}$ and $\Delta[Ca]_{den}$, respectively) (Figure 1C). Analysis was limited to spines with clearly defined heads that were well separated from the parent dendrite and located less than 150 μm from the soma on radial oblique dendrites.

Activation of mAChRs Enhances Synaptic Potentials and Ca Transients

Uncaging-evoked potentials and Ca transients were measured in control conditions and in the presence of the broad spectrum mAChR agonist oxotremorine-m (oxo-m, 1 μM) (Figure 1D). In the presence of oxo-m, both the uEPSP and $\Delta[Ca]_{spine}$ were significantly increased (n = 32; uEPSP: 1.51 ± 0.12 mV; spine $\Delta G/G_{sat}$: 14.0% ± 0.89%; dendrite $\Delta G/G_{sat}$: 2.24% ± 0.22%) relative to control (n = 30; uEPSP: 0.87 ± 0.10 mV, $p < 0.05$; spine $\Delta G/G_{sat}$: 7.73% ± 0.54%, $p < 0.05$; dendrite $\Delta G/G_{sat}$: 2.14% ± 0.22%, $p = 0.25$) (Figure 1D). These changes were prevented by incubation in the general mAChR antagonist scopolamine (10 μM) (n = 15; uEPSP: 0.83 ± 0.13 mV, $p < 0.05$; spine $\Delta G/G_{sat}$: 8.99% ± 0.52%, $p < 0.05$; dendrite $\Delta G/G_{sat}$: 0.86% ± 0.20%, $p < 0.05$, relative to oxo-m), indicating that the enhancement of synaptic responses by oxo-m resulted from activation of muscarinic receptors. Furthermore, in the presence of the M1 muscarinic receptor antagonist muscarinic toxin 7 (Mtx-7, 100 nM), synaptic responses were unaffected by the additional application of oxo-m (n = 19, 1.02 ± 0.14 mV in Mtx-7 versus n = 18, 1.048 ± 0.12 mV in Mtx-7 + oxo-m, $p = 0.89$; $\Delta G/G_{sat}$: 7.59% ± 0.62% in Mtx-7 and 8.21% ± 0.71% in Mtx-7 + oxo-m, $p = 0.51$), indicating that enhancement of synaptic potentials and Ca influx were due to activation of M1 receptors (Figures 1E and 1F). As expected from the modulation of K channels by activation of muscarinic receptors, the membrane resistance of the neuron was increased by oxo-m and these changes were also prevented by Mtx-7 (see Table S1 and Figure S1 available online for a summary of passive membrane properties and uncaging laser power for all conditions).

The Intrinsic Properties and Numbers of Glutamate Receptors Are Not Directly Altered by mAChR Activation

The increase in uEPSP and $\Delta[Ca]_{spine}$ induced by mAChR activation might result from the modulation of the number or properties of AMPARs and NMDARs or indirectly as a result of increased membrane resistance. We tested these possibilities by examining uncaging-evoked postsynaptic currents (uEPSCs) and Ca transients in voltage-clamped neurons filled with a cesium-based internal and bathed in a cocktail of voltage-sensitive channel antagonists (ω-conotoxin-MVIIC, SNX-482, nimodipine, and mibefradil and tetrodotoxin (TTX) to block $Ca_V2.1$, $Ca_V2.2$, $Ca_V2.3$, $Ca_V1.2/1.3$, $Ca_V3.1/3.2/3.3$, and voltage-sensitive Na channels; see Experimental Procedures) (Figure 2). This approach allowed us to measure the small AMPAR- and NMDAR-mediated currents resulting from activation of a single postsynaptic terminal without contributions from voltage-gated ion channels that are present in dendrites and spines. Note that under these conditions the membrane resistance is significantly increased and, by limiting analysis to spines in the proximal dendrite, voltage- and space-clamp quality is high. Neurons were voltage clamped at a potential of −70 mV in order to measure AMPAR-mediated uEPSCs and NMDAR-mediated Ca influx and subsequently depolarized to +40 mV to measure

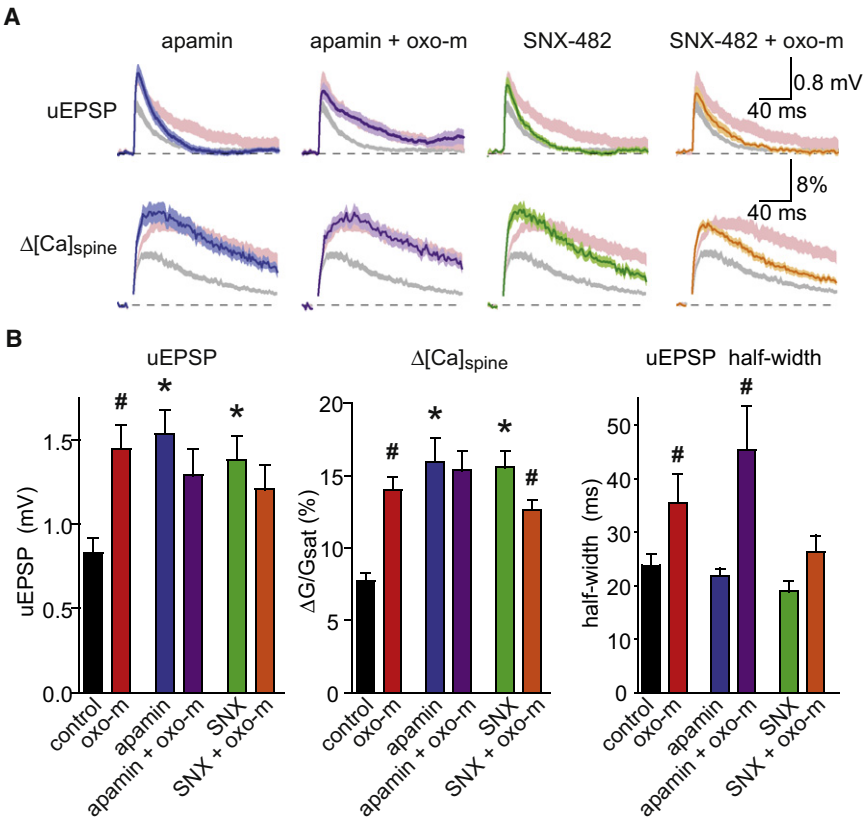

Figure 3. The Effects of mAChR Activation on Synaptic Potentials and Ca Influx Are Mimicked and Occluded by Antagonism of $Ca_V2.3$ or SK Channels

(A) uEPSPs (top) and $\Delta[Ca]_{spine}$ (bottom) measured in the presence of apamin (far left, blue), apamin + oxo-m (left, purple), SNX-482 (right, green), and SNX-482 + oxo-m (far right, orange). The ranges of responses measured in control conditions and in the presence of oxo-m are shown for comparison in shaded gray and pink, respectively.

(B) Summary of amplitudes of uEPSPs (left), $\Delta[Ca]_{spine}$ (middle), and uEPSP half-width (right) measured in the conditions shown in (A). For conditions without oxo-m, (*) indicates a significant difference from control ($p < 0.05$). For conditions with oxo-m, (#) indicates a significant difference between the indicated condition and the same without oxo-m ($p < 0.05$).

NMDAR-mediated uEPSCs (Figure 2A). Relative to control conditions, activation of mAChRs did not significantly alter the uEPSCs at either −70 (−13.97 ± 1.30 and −13.35 ± 1.19 pA in control [n = 19] and oxo-m [n = 21], respectively; p = 0.73) or +40 mV (3.75 ± 0.69 and 3.06 ± 0.84 pA; p = 0.52) (Figure 2B). Similarly, $\Delta[Ca]_{spine}$ and $\Delta[Ca]_{den}$ were unaffected at −70 mV (spine $\Delta G/G_{sat}$: 23.08% ± 2.70% and 25.78% ± 3.43%, p = 0.54; dendrite $\Delta G/G_{sat}$: 5.41% ± 0.88% and 7.83% ± 1.54%, p = 0.19, control versus oxo-m) and at +40 mV (spine $\Delta G/G_{sat}$: 55.36% ± 6.32% and 49.85% ± 6.33%, p = 0.54, dendrite $\Delta G/G_{sat}$: 18.43% ± 3.70% and 20.50% ± 4.29%, p = 0.72, control versus oxo-m). Furthermore, the lack of modulation of uEPSCs measured at the soma is unlikely to result from poor voltage or space clamp because Ca transients measured in the spine were also unaffected. Had there been differential loss of voltage-clamp across conditions, this would have resulted in differences in membrane potential at the spine and thereby strong modulation of NMDAR-dependent Ca influx (Bloodgood et al., 2009; Grunditz et al., 2008).

Thus, activation of mAChRs does not directly enhance ionic currents or Ca influx through AMPARs or NMDARs and also does not directly boost Ca influx through NMDARs. Therefore, the enhanced synaptic potentials and Ca influx seen following mAChR activation cannot be explained by modulation of the numbers or biophysical properties of ionotropic glutamate receptors.

The Effects of mAChRs Are Mimicked and Occluded by Blockade of $Ca_V2.3$ Voltage-Gated Ca Channels or SK-Type Ca-Activated K-Channels

In hippocampal CA1 pyramidal neurons, synaptic potentials and Ca influx are inhibited by a nonlinear ionic signaling cascade that is triggered in individual active spines (Bloodgood et al., 2009; Bloodgood and Sabatini, 2007; Ngo-Anh et al., 2005). In brief, opening of glutamate receptors depolarizes the active spine, activating $Ca_V2.3$ channels, which flux Ca that activates SK channels. SK channels repolarize the spine or shunt depolarizing currents and thereby truncate synaptic potentials and Ca influx. We used whole-cell current-clamp recordings to examine if components of this feedback system were necessary for mAChR-induced enhancements of synaptic potentials and Ca influx (Figure 3). Consistent with previous studies, blocking SK channels with apamin (100 nM) enhanced the peak uEPSP (n = 22; 1.54 ± 0.14 mV, $p < 0.05$) and $\Delta[Ca]_{spine}$ ($\Delta G/G_{sat}$ = 15.9% ± 1.6%, $p < 0.05$) relative to control, thus mimicking the effects of oxo-m. Additionally, incubation in apamin prevented the effects of oxo-m such that uEPSP and $\Delta[Ca]_{spine}$ in this condition were unaffected by activation of mAChRs (n = 18; uEPSP; 1.30 ± 0.16 mV, p = 0.25; spine $\Delta G/G_{sat}$; 15.4% ± 1.35%, p = 0.79, compared with apamin alone). Similarly, blocking $Ca_V2.3$ with the peptide toxin SNX-482 (300 nM) mimicked the effects of oxo-m on the amplitudes of the uEPSP and $\Delta[Ca]_{spine}$ (n = 19; uEPSP: 1.39 ± 0.14 mV, $p < 0.05$; spine $\Delta G/G_{sat}$: 15.56% ± 1.11%, $p < 0.05$; compared with control). Furthermore, in the presence of SNX-482, the additional application of oxo-m failed to increase and instead slightly decreased each synaptic parameter (n = 23; uEPSP: 1.21 ± 0.15 mV, p = 0.34; spine $\Delta G/G_{sat}$: 12.62% ± 0.68%, $p < 0.05$, compared with SNX-482 alone) (Figures 3A and 3B). Activation of mAChRs also increased the half-width of the uEPSP in control conditions and in the presence

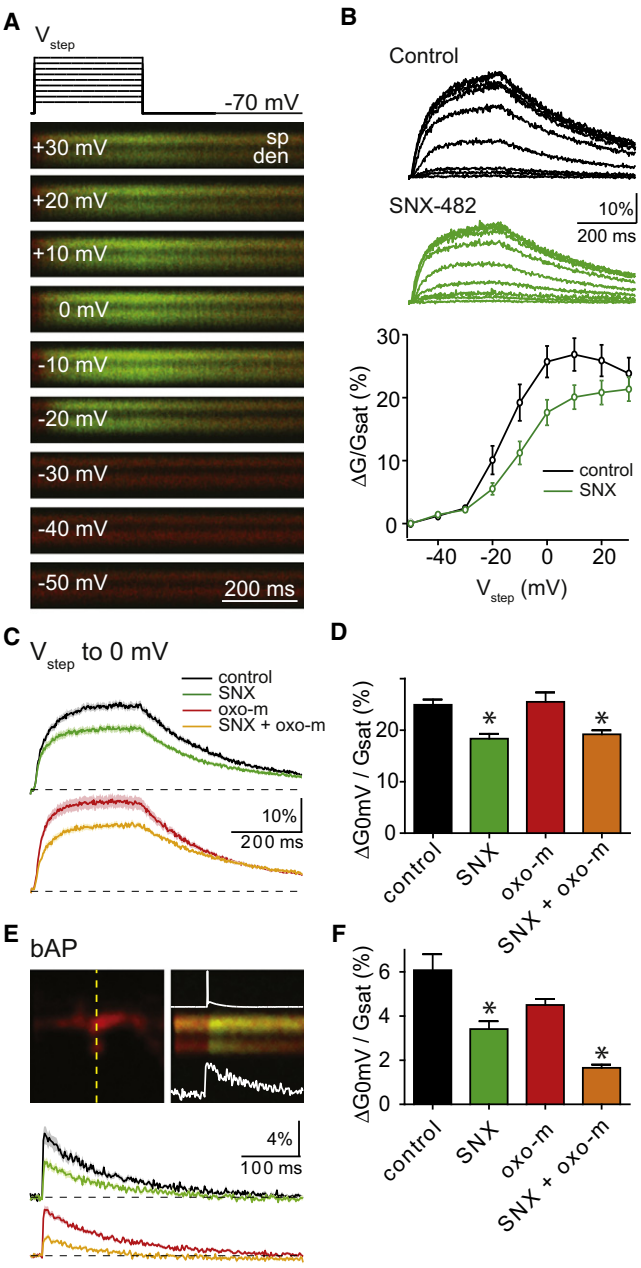

Figure 4. Activation of mAChRs Does Not Enhance $Ca_V2.3$-Mediated Ca Influx into Active Spines

(A) Top: voltage-step protocol showing 300 ms steps to −50, −40, −30, −20, −10, 0, +10, +20 and +30 mV from a holding potential of −70 mV. Bottom: Example series of fluorescence transients evoked by steps to the indicated potentials measured in line scans intersecting a spine head (sp) and neighboring dendrite (den).

(B) Top: average fluorescence transients measured as in (A) showing depolarization-dependent Ca influx into the spine head in control (black) and in the presence of SNX-482 (green). Bottom: summary data for $\Delta[Ca]_{spine}$ measured as in (A) in control (black) and SNX-482 (green).

(C) Top: average fluorescence transients for voltage steps to 0 mV in control (black) and SNX-482 (green). Bottom: as above, but in the presence of oxo-m (red) and SNX-482 + oxo-m (orange).

(D) Summary of $\Delta G/G_{sat}$ in response to voltage steps to 0 mV measured in the four pharmacological conditions shown in (C). (*) indicates significantly different from the corresponding SNX-482-lacking condition.

(E) Image of a spine and dendrite (top, left) and an example of fluorescence collected during line scan (top, right) indicated by the dashed yellow line. Overlaid on the line scan fluorescence image is the action potential recorded at the soma (top) and the quantification of the $\Delta G_{bAP}/G_{sat}$ from the spine head (bottom). Bottom: average $\Delta G_{bAP}/G_{sat}$ from the spine head measured in control (black), SNX-482 (green), oxo-m (red), and oxo-m + SNX-482 (orange).

(F) Summary of $\Delta G_{bAP}/G_{sat}$ amplitude for the four pharmacological conditions shown in (D). (*) indicates significantly different from the corresponding SNX-482-lacking condition.

of apamin, but not when $Ca_V2.3$ channels were antagonized (Figures 3A, 3B, and S2), suggesting a central role of $Ca_V2.3$ channels in controlling the duration of the synaptic potential when mAChRs are activated. Lastly, oxo-m altered the kinetics of the spine $\Delta G/G_{sat}$ by delaying the peak and decay phase of the transients, consisted with prolonged Ca influx following activation of mAChRs (Figure S2). This effect was not seen when either SK or $Ca_V2.3$ channels were blocked (Figure S2).

Taken together, these results suggest that the mechanisms of enhancement of synaptic responses by activation of mAChRs, blockade of $Ca_V2.3$ channels, and blockade of SK channels share common elements. Furthermore, they suggest that the mechanism of the postsynaptic effects of mAChR activation may be inhibition of either $Ca_V2.3$ or SK channels. Lastly, although increased membrane resistance may also contribute to the enhancement of synaptic potentials seen following activation of mAChRs, the lack of synaptic enhancement when $Ca_V2.3$ or SK channels are blocked indicates that this effect is likely minor.

Activation of mAChRs Does Not Modulate $Ca_V2.3$-Mediated Ca Influx into Dendritic Spines

Somatic currents mediated by $Ca_V2.3$ channels have been reported to be enhanced by mAChR agonists (Tai et al., 2006). However, these studies did not examine if mAChRs regulate $Ca_V2.3$-mediated Ca influx into spines. To answer this question, we monitored spine and dendrite Ca transients evoked by a series of 300 ms voltage steps from −70 mV to depolarized potentials (Figure 4). These recordings were performed with Cs and tetraethylammonium (TEA) in the intracellular solution and in the presence of a cocktail of ion channel antagonists (ω-conotoxin-MVIIC, nimodipine, TTX, picrotoxin, NBQX, CPP, CsCl, and 4-Aminopyridine (4AP) to block $Ca_V2.1$, $Ca_V2.2$, $Ca_V1.2$/1.3, voltage-sensitive Na channels, $GABA_A$ receptors, AMPARs, NMDARs, and K channels, respectively) in order to better isolate $Ca_V2.3$-mediated Ca influx. Note that antagonists of $Ca_V3.X$ channels such as mibefradil and Ni^{2+} also at least partially block $Ca_V2.3$ and were therefore not included (Randall and Tsien, 1997). Depolarization generated large Ca transients in the spine and neighboring dendrite that decayed following repolarization to −70 mV (Figure 4A). In control conditions (n = 18), the magnitude of the spine head Ca transient was relatively small for steps to less than −30 mV, but increased steadily in the range of −30 to 0 mV (Figures 4A–4C), consistent with the known voltage-activation curve of $Ca_V2.3$ channels in these cells (Randall and Tsien, 1997; Tai et al., 2006). Application of SNX-482 (n = 24) reduced

the spine Ca influx in the same voltage range, demonstrating contributions of $Ca_V2.3$ channels to depolarization-evoked Ca influx (Figure 4B).

In test experiments we found that despite the extensive blockade of voltage-gated ion channels, application of oxo-m still increased the membrane resistance (from 261 ± 21 MΩ in control to 361 ± 21 with oxo-m, $p < 0.05$), which might alter the ability of somatic step depolarizations to control the potential in the spine. This might result from modulation of two-pore K channels such as TASK channels, which have been described to be regulated by G_q-coupled receptors and are one of the few K channels insensitive to the presence of intracellular Cs and TEA and extracellular Cs and 4AP (Millar et al., 2000; Taverna et al., 2005). Therefore, we examined the effects of oxo-m and SNX-482 application on spine Ca transients evoked by voltage steps to 0 mV in the additional presence of extracellular 3 mM $BaCl_2$ (Figures 4C and 4D). Under these conditions, application of oxo-m had no significant effect on membrane resistance (286 ± 16 and 336 ± 31 MΩ for control, n = 23 and oxo-m, n = 21, respectively, $p = 0.15$). However, application of SNX-482 (n = 22) reduced the step-evoked Ca influx by ~26% (24.9% ± 1% $\Delta G/G_{sat}$ in control versus 18.4% ± 1% in SNX-482; $p < 0.05$), confirming the contribution of these channels to depolarization-evoked Ca influx into the spine. The remaining Ca influx is likely due to spine $Ca_V3.X$ and an unblocked, uncharacterized voltage-gated calcium channel (VGCC), as well as to the fact that SNX-482 is not a pore blocker of $Ca_V2.3$, but rather an allosteric modulator that shifts activation to more depolarized potentials (Bloodgood et al., 2009; Bloodgood and Sabatini, 2007; Bourinet et al., 2001).

Application of oxo-m had no effect on step-evoked Ca influx in control conditions ($\Delta G/G_{sat}$: 25.5% ± 1.8%, n = 21) or in the presence of SNX-482 ($\Delta G/G_{sat}$: 19.18% ± 0.7%, n = 19), indicating that mAChR activation does not regulate voltage-gated Ca channels in the dendritic spine. Furthermore, the kinetics of Ca clearance were unaffected by oxo-m as determined from the decay time constant of the fluorescent transients (224 ± 14 ms and 218 ± 14 ms, control versus oxo-m).

In a parallel set of experiments in artificial cerebrospinal fluid (ACSF) with apamin, nimodipine, ω-conotoxin-MVIIC, NBQX, and CPP to block SK, $Ca_V1.2/1.3$, $Ca_V2.1/2.2$, AMPARs, and NMDARs, respectively, and K-based intracellular solution, back-propagating action potentials (bAPs) triggered by somatic current injection were used to activate voltage-gated Ca channels in the spine and dendrite and examine possible regulation of $Ca_V2.3$ (Figures 4E and 4F). Apamin was included to block SK-type Ca-activated K channels, which are present in the spine and may indirectly influence bAP-evoked Ca influx (Bloodgood and Sabatini, 2007; Ngo-Anh et al., 2005). In these conditions, oxo-m reduced the magnitude of bAP-evoked Ca influx ($\Delta G_{bAP}/G_{sat}$: 6.1% ± 0.7%, n = 23, control versus 4.5% ± 0.3%, n = 21, oxo-m). This effect may result from changes in the dendritic membrane potential, changes in the action potential waveform, or modulation of dendritic ion channels. Nevertheless, application of SNX-482 reduced bAP-evoked Ca influx further in control conditions and in the presence of oxo-m, indicating that $Ca_V2.3$ channels are active under both conditions. The magnitude of the SNX-482-sensitive component was unaffected by application of oxo-m, providing independent support that these channels are not strongly modulated by mAChR activation (2.7% ± 0.81% and 2.85% ± 0.31% $\Delta G/G_{sat}$ in control and oxo-m, respectively). The decay kinetics of the bAP-evoked Ca transient were unaffected by oxo-m (control: 129 ± 8 ms, oxo-m: 133 ± 9 ms, SNX-482: 111 ± 13 ms, SNX-482 + oxo-m: 105 ± 12 ms), confirming a lack of effect of mAChR activation on Ca handling in the spine.

Activation of mAChRs Inhibits Opening of SK Channels by Reducing Their Ca Sensitivity

Since $Ca_V2.3$ channels in spines were unaffected, we examined if mAChR activation inhibited SK channels (Figure 5). These experiments were done using a K-based internal solution, without the addition of ion channel antagonists, and at a holding potential of −50 mV. Voltage steps (200 ms) to +60 mV activate voltage-gated Ca channels and, on repolarization to −50 mV, trigger outward currents that are at least partially mediated by Ca-activated K channels (Figure 5A) (Sah and Isaacson, 1995; Stackman et al., 2002). We found that these repolarization-evoked currents were robustly inhibited by apamin, indicating that they were primarily due to SK channels (Figures 5A and 5B) (n = 8; baseline: 40.62 ± 6.99 pA; apamin: −7.23 ± 3.74 pA, $p < 0.05$). In contrast, in the presence of oxo-m, repolarization-evoked currents were reduced relative to control and showed little sensitivity to apamin application (n = 7; baseline: −9.94 ± 9.26 pA; apamin: −21.25 ± 5.88 pA, $p = 0.19$) (Figures 5A–5C). The total apamin-sensitive charge transfer was nearly eliminated by activation of mAChRs (Figure 5D, control: 7.94 ± 1.04 pC and oxo-m: 0.90 ± 1.57 pC, $p < 0.05$). Under these conditions, the kinetics of the apamin-sensitive current in control conditions had a decay tau of 417 ± 134 ms, slower than the off-rate of Ca from SK channels, but consistent with previously reported voltage-step activation of Ca-activated K currents (Bildl et al., 2004; Sah and Isaacson, 1995). Unfortunately, the small size of the apamin-sensitive current in the presence of oxo-m prevented accurate measurement of its kinetics following mAChR activation.

The reduction of SK currents with mAChR activation could be due to several possible effects on SK channels, including their internalization from the membrane, a shift in their Ca sensitivity, or a their decoupling from VGCCs (Faber et al., 2008; Lin et al., 2008; Maingret et al., 2008). Alterations in space-clamp due to the effects of mAChR activation on input resistance can make distinguishing these possibilities difficult. Therefore, we activated SK-mediated currents directly by uncaging Ca intracellularly (Figure 6). Neurons were voltage clamped at −50 mV and filled through the patch pipette with a K-based internal solution containing NP-EGTA (2 mM), a Ca chelator that is photolyzed by ultraviolet (UV) light (Ellis-Davies and Kaplan, 1994; Schneggenburger and Neher, 2000). Under these conditions, 355 nm UV laser flashes (50 ms) directed to a ~250 μm diameter area in the apical dendrite elicited inward currents that were largely blocked by apamin (Figures 6A–6C). Apamin-sensitive currents could also be evoked in the presence of oxo-m (Figures 6B and 6C), indicating that SK channels were still present at the plasma membrane and could be opened by increases in intracellular Ca. Under these conditions, SK channels are activated by

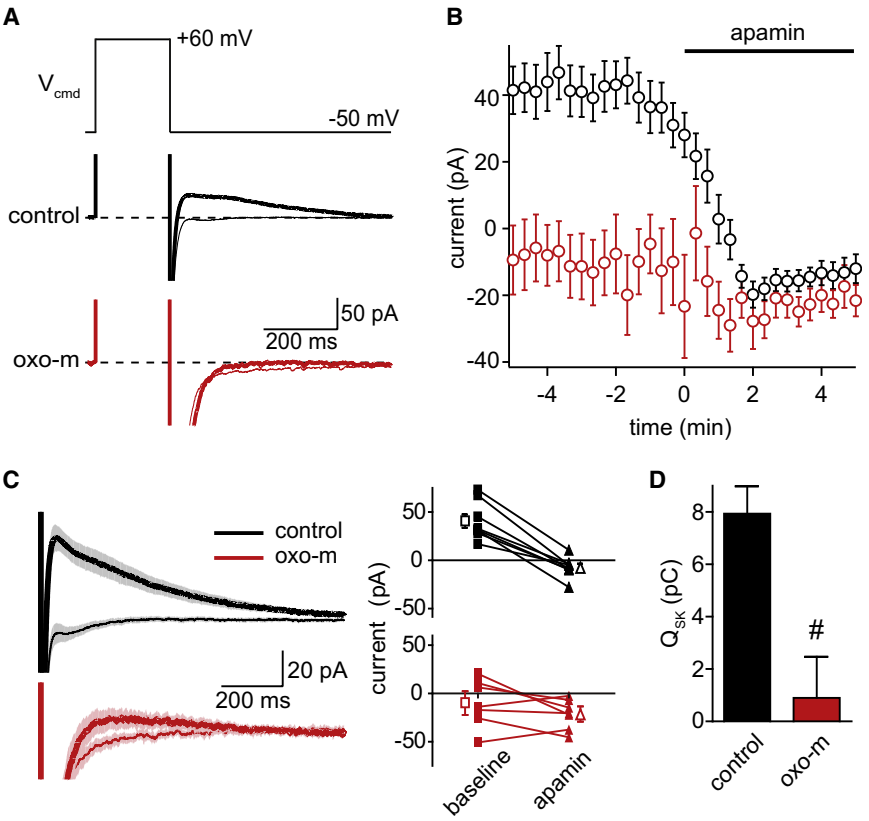

Figure 5. Activation of mAChRs Inhibits Repolarization-Evoked SK Currents

(A) Voltage-step protocol (top) used to activate voltage-gated Ca channels, which leads to the accumulation of intracellular Ca and activation of Ca-activated K currents (bottom). Examples of currents measured in control conditions (black) and in the presence of oxo-m (red) before (thick lines) and after (thin lines) the application of apamin are shown.

(B) Summary of the time courses of the effects of apamin on repolarization-evoked current amplitudes in control conditions (black) and in the presence of oxo-m (red).

(C) Average currents evoked by repolarization (left) and summary of effects of apamin on current amplitudes in individual cells (right) in control conditions (black) and in oxo-m (red). Thick and thin traces depict currents in the baseline period and after application of apamin, respectively.

(D) Summary of apamin-sensitive repolarization-evoked charge transfer measured in control conditions (black) and in oxo-m (red).

a spatially homogenous and large Ca transient within the uncaging spot. Clearance of Ca is slowed by the large concentration of Ca buffer (2 mM NP-EGTA) and therefore the kinetics of the SK current are dominated by Ca clearance and much slower than when the channel is activated by Ca increases in the microdomain of an active VGCC. For this reason, we find that the time constant of decay of the Ca uncaging-evoked current is slower (time constant 330 ± 65 ms in control and 566 ± 154 ms in the presence of oxo-m) than that of current carried by SK channels expressed in inside-out patches probed with rapid Ca exchanges (Bildl et al., 2004).

To test if the Ca sensitivity of SK channels was altered by activation of mAChRs, we repeated the analysis of Ca-uncaging evoked currents using a fixed laser power and uncaging spot while varying laser pulse length from 2 to 50 ms. In control conditions (n = 9), these pulses generated a family of outward currents whose magnitude increased gradually for pulse durations between 5 and 20 ms (Figures 6D and 6E). In the presence of oxo-m (n = 11), the amplitudes of these outward currents were reduced for pulse lengths of 5–15 ms but unaffected for longer pulses (Figures 6D and 6E). The amplitudes of evoked currents were well described in both conditions as sigmoidal functions of pulse duration (Figure 6E). The fit parameters of maximum amplitude, midpoint, and rate were 99.6 ± 2.5 pA, 9.7 ± 0.4 ms, and 2.6 ± 0.2 in control; and 100.8 ± 4.2 pA, 14.6 ± 0.5 ms, and 3.4 ± 0.2 in oxo-m. The rightward shift of the fit in oxo-m relative to that in control indicates a reduction in the sensitivity of the channel to intracellular Ca.

SK Inhibition Occurs in the Spine and Requires CK2

Previous studies in heterologous systems and somatic patches from sympathetic superior cervical ganglion neurons demonstrated that the Ca sensitivity of SK opening is modulated by phosphorylation of a bound calmodulin molecule by CK2 (Bildl et al., 2004; Maingret et al., 2008). Furthermore, previous studies have demonstrated that SKs are present in dendritic spines where their activation due to synaptically evoked Ca influx limits the amplitude of EPSPs (Faber et al., 2005; Ngo-Anh et al., 2005).

In order to determine if the regulation of SK by mAChRs is mediated by CK2 and if it occurs specifically in the spine we carried out two additional sets of experiments (Figure 7). EPSPs evoked by stimulation of Schaffer collaterals are enhanced by blockade of SK channels with apamin in an NMDA receptor and extracellular Mg dependent manner (Ngo-Anh et al., 2005). Under conditions of weak synaptic stimulation or focal activation of a single spine with glutamate uncaging, the SK channels that are opened must be located on the active spine because synaptically-evoked Ca accumulation only occurs within the spine head (Sabatini et al., 2002). Therefore, if mAChR activation inhibits opening of SK channels in the spine, one would predict that activation of mAChRs would prevent the effects of apamin on EPSPs evoked by Schaffer collateral stimulation. We found that in control conditions, application of apamin increased the amplitude of the EPSP by on average ~58% (n = 8, 5.13 ± 0.31 to 8.1 ± 0.41 mV, $p < 0.05$), consistent with previous reports (Ngo-Anh et al., 2005) (Figures 7A–7C). In contrast, in the presence of oxo-m, apamin flow-in had no effect on EPSP amplitude (n = 8, 5.0 ± 0.52 mV to 5.33 ± 0.64 mV, $p = 0.47$), consistent with prior inhibition of spine SK channels due to mAChR activation. Lastly, examination of the effects of oxo-m on synaptic signals in the presence of the CK2 antagonist

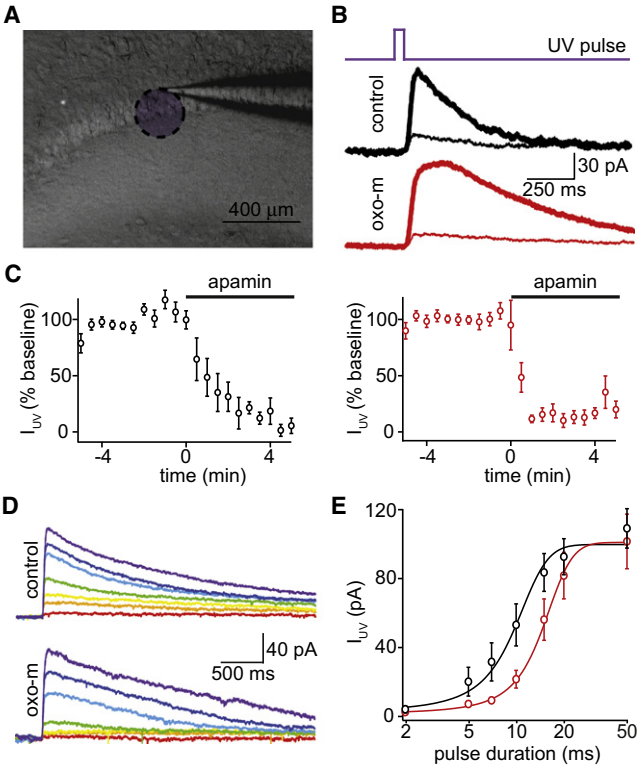

Figure 6. Activation of mAChRs Reduces the Ca Sensitivity of SK Channels

(A) Low-magnification gradient contrast image (gray) of the hippocampus slice showing the recording electrode with an overlay (purple) indicating the approximate area exposed to UV light.

(B) Timing of UV laser pulse (top), and examples of UV light-evoked currents (I_{UV}) measured in control conditions (middle) and in oxo-m (bottom). Currents are shown for the baseline period (thick lines) and after application of apamin (thin traces).

(C) Summary of the time courses of the effects of apamin application on the peak of UV-evoked currents in control conditions (black, left) and in the presence of oxo-m (red, right).

(D) Average currents evoked by UV laser pulses of a variety of durations in control conditions (top) and in oxo-m (bottom). Colors correlate with increasing duration of UV uncaging pulse (red to purple; 2, 5, 7, 10, 15, 20, and 50 ms).

(E) Summary of the peak amplitudes of UV-evoked currents as a function of laser pulse duration measured in control conditions (black) and in the presence of oxo-m (red). The lines depict the best fits to the data using sigmoidal functions.

4,5,6,7-Tetrabromobenzotriazole (TBB, 10 µM) demonstrated that TBB prevented the effects of mAChR activation on both uEPSPs (0.99 ± 0.1 and 0.83 ± 0.1 mV, TBB versus TBB + oxo-m) and spine Ca transients (7.5% ± 0.5% and 8.09% ± 0.9% $\Delta G/G_{sat}$, TBB versus TBB + oxo-m) (Figures 7D and 7E). Therefore, our results indicate that activation of mAChRs regulates synaptic potentials and Ca influx via a pathway that both requires activity of CK2 and inhibits SK channels present in dendritic spines.

DISCUSSION

Here we use optical and electrophysiological approaches to isolate and examine the postsynaptic effects of mAChR activation on glutamatergic transmission in CA1 pyramidal neurons in acute slices of juvenile mouse hippocampus. We find that mAChRs increase the amplitude and duration of synaptic potentials resulting from activation of individual postsynaptic terminals, as well as the amplitude of corresponding synaptic Ca transients in active spines. The effects are mediated by activation of M1-type muscarinic receptors and require signaling through CK2. Furthermore, these effects require opening of SK-type Ca-activated K channels and $Ca_V2.3$ voltage-gated Ca channels and are mediated by inhibition of SK in dendritic spines.

The current study describes mAChR-induced changes in synaptic responses elicited by activation of a single postsynaptic terminal. It is not possible to directly compare our results to the effects on unitary or compound synaptic responses, which are influenced by effects of mAChRs on vesicular release probability and on the integrative properties of the postsynaptic neuron. Furthermore, we specifically examined postsynaptic terminals of synapses formed onto large-head dendritic spines, which are characterized functionally by relatively high AMPAR content and high probability of release and anatomically by large-area postsynaptic densities and presynaptic active zones (Harris and Stevens, 1989; Matsuzaki et al., 2001; Oertner et al., 2002; Schikorski and Stevens, 1997). Responses from these spines likely dominate synaptic responses triggered by extracellular stimulation of Schaffer collaterals and such spines display robust NMDAR-dependent LTP following a variety of induction protocols (Harvey and Svoboda, 2007; Harvey et al., 2008; Steiner et al., 2008; but see Matsuzaki et al., 2004).

Regulation of SK Channels

SK channels are widely expressed in the brain and are found in dendritic spines associated with CA3 to CA1 synapses (Ngo-Anh et al., 2005). SK channels exist in a complex with calmodulin, which confers onto the channel its Ca sensitivity, and also with the serine/threonine kinase CK2 and protein phosphotase 2A (PP2A), which regulate the Ca sensitivity of the channel (Allen et al., 2007; Keen et al., 1999; Xia et al., 1998). CK2 phosphorylation of SK-bound calmodulin shifts the EC_{50} for SK opening by Ca from ~0.4 mM to ~1.4 mM (Bildl et al., 2004; Maingret et al., 2008). Since bulk-average synaptically evoked Ca transients in active dendritic spines only reach ~1 µM (Sabatini et al., 2002), the high EC_{50} of SK activation by Ca is consistent with their localization within the Ca nanodomain of voltage-gated Ca channels such as $Ca_V2.3$. In the hippocampus, SK opening is inhibited by activation of the sigma receptor, a PLC-coupled GPCR (Martina et al., 2007). Furthermore, several GPCRs modulate a previously unidentified Ca-activated K current in these cells (Sah and Isaacson, 1995). Here we demonstrate that blocking SK channels mimics and occludes the effects of oxo-m on responses from individual CA1 glutamatergic postsynaptic terminals and that oxo-m reduces repolarization-evoked SK currents. Furthermore, we show that mAChR activation reduces the sensitivity of SK channels to increases in intracellular Ca released by UV uncaging, consistent with the actions of CK2. Lastly, we show that the CK2 antagonist TBB prevents the effects of oxo-m on synaptic potentials and Ca transients. CK2 has been previously shown to act downstream of norepinephrine receptors in

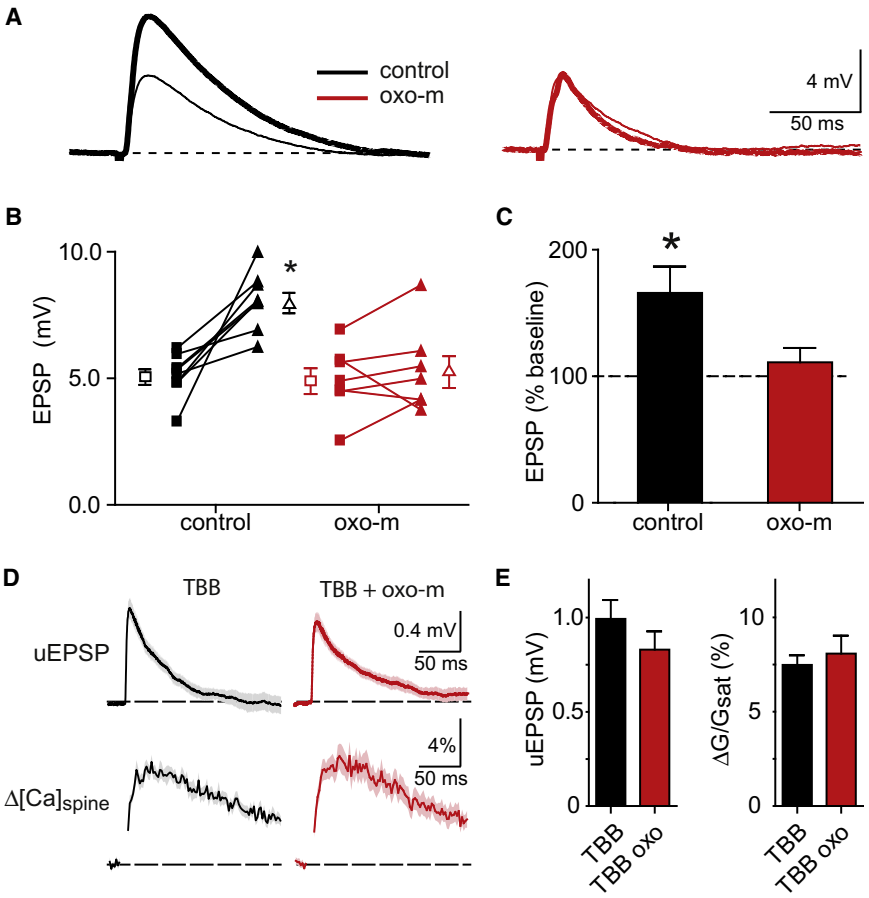

Figure 7. mAChR-Dependent Inhibition of SK Occurs in the Spine and Requires CK2

(A) Example of EPSPs evoked by Schaffer collateral stimulation before (thin lines) and after (thick lines) application of 100 nM apamin in control conditions (black) and in the presence of oxo-m (red).

(B) Summary of the effects of apamin application on EPSP amplitude (connected closed symbols) for each cell in control conditions (black) and in the presence of oxo-m (red). The average EPSP amplitude is also shown in each condition (open symbols).

(C) Summary of the relative amplitude of the EPSP after apamin application compared with baseline for control conditions (black) and in the presence of oxo-m (red). (*) indicates significantly different than 100%.

(D) uEPSPs (top) and $\Delta[Ca]_{spine}$ (bottom) measured in the presence of TBB (left, black) and TBB + oxo-m (right, red).

(E) Summary of the uEPSP and $\Delta G/G_{sat}$ amplitudes for the conditions shown in (D).

superior cervical ganglion neurons to phosphorylate SK-associated calmodulin (Maingret et al., 2008).

SK channels are also regulated by PKA, whose activity triggers their internalization and enhances synaptic potentials (Faber et al., 2008; Lin et al., 2008). Though our results do not specifically rule out a role of PKA in the effects described here, we do not believe that SK internalization makes a significant contribution because the maximum amplitudes of SK currents triggered by intracellular Ca uncaging were unaffected by mAChR activation. Furthermore, the effects that we demonstrate require M1 mAChRs, which couple to PLC via $G_{\alpha q}$ and not to PKA via $G_{\alpha s}$ or $G_{\alpha i}$ (Levey et al., 1995; Rouse et al., 1999, 2000). Thus, our data and published results support a model in which activation of the $G_{\alpha q}$-coupled M1 mAChRs activate CK2 that phosphorylates calmodulin bound to SK channels, thereby preventing synaptic activation of SK in the spine and hence derepressing synaptic potentials and Ca influx.

Lack of Regulation of Spine $Ca_V2.3$ Channels

VGCCs are common downstream targets of GPCR modulation (Catterall, 2000). In CA1 pyramidal neurons of the rat, mAChR activation enhances somatic $Ca_V2.3$ by shifting the activation curve to more hyperpolarized potentials via a Ca-insensitive PLC-dependent pathway (Tai et al., 2006). Importantly, Tai et al. did not block two-pore K channels such as TASK that our data suggests mediate much of the effect of mAChRs on input resistance. We find that in CA1 pyramidal neurons of the mouse, when VGCCs are activated by step depolarizations in the presence of extracellular $BaCl_2$ or by bAPs, the SNX-482-sensitive component of spine Ca influx is not regulated by mAChRs. Based on their activation voltages and pharmacological profile, these channels likely correspond to the α_{1e} encoded or $Ca_V2.3$ voltage-gated Ca channel (Catterall et al., 2005). Despite the lack of a direct modulation of these channels, $Ca_V2.3$ opening contributes to the effects of mAChRs on the synaptic potentials because the oxo-m-induced increase in the duration of synaptic potentials was prevented by blockade of $Ca_V2.3$, but not of SK.

Control of Synaptic Signals by Ca-Gated Ion Channels in Active Spines

Recent work has demonstrated the presence of a nonlinear and negative feedback loop that is engaged in individual active spines of CA1 pyramidal neurons and that normally suppresses synaptic potentials and Ca influx (Bloodgood et al., 2009; Bloodgood and Sabatini, 2007; Ngo-Anh et al., 2005). In this model, synaptic depolarization activates $Ca_V2.3$ channels located in the spine. In turn, Ca influx through $Ca_V2.3$ activates SK channels, which hyperpolarize the spine or shunt depolarizing currents, thereby truncating the synaptic depolarization and reducing NMDAR-mediated Ca influx by promoting Mg block of the receptor.

In principal, mAChR-dependent enhancement of synaptic potentials and Ca influx could have occurred via enhancement of AMPAR and NMDAR currents, via inhibition of $Ca_V2.3$, or via inhibition of SK. We find that ionotropic glutamate receptors are not directly affected such that under high-quality voltage-clamp with inhibition of voltage- and Ca-gated channels, AMPAR and NMDAR currents and NMDAR Ca influx are

unaffected by mAChRs. Instead, the effects of mAChR activation on the amplitude and duration of synaptic potentials as well as on synaptic Ca influx result from the regulation a downstream element of the feedback loop. Given the multiple regulatory mechanisms that target $Ca_V2.3$, SK, calmodulin, PKA, PLC, and PP2A, it is likely that other neuromodulators also affect synaptic responses by regulating this signaling loop.

Conclusion

Our results demonstrate that postsynaptic M1 mAChRs regulate synaptic responses resulting from activation of individual postsynaptic terminals at CA3 to CA1 synapses. These effects do not require regulation of ionotropic glutamate receptors and, instead, are mediated by inhibition of SK channels in dendritic spines. This mode of regulation results in large (~2-fold) enhancements of synaptic potentials and Ca influx that, in turn, are expected to promote the induction of NMDAR-dependent forms of LTP in vitro and the acquisition of hippocampal-dependent behaviors in vivo.

EXPERIMENTAL PROCEDURES

Animal Handling and Slice Preparation

Animals were handled according to protocols that were approved by the Harvard Standing Committee on Animal Care and that are in accordance with federal guidelines. Postnatal day 15–18 C57/Bl6 mice were anesthetized by inhalation of isoflurane. Transverse hippocampal slices were prepared as described previously (Bloodgood and Sabatini, 2007) in a cold choline-based ACSF containing (in mM) 25 $NaHCO_3$, 1.25 NaH_2PO_4, 2.5 KCl, 7 $MgCl_2$, 25 glucose, 1 $CaCl_2$, 110 choline chloride, 11.60 ascorbic acid, and 3.10 pyruvic acid, and equilibrated with 95% O_2/5% CO_2. Slices of 300 μm thickness were cut with a Leica VT1000s (Leica Instruments, Nussloch, Germany) and transferred to a holding chamber containing ACSF consisting of (in mM) 127 NaCl, 2.5 KCl, 25 $NaHCO_3$, 1.25 NaH_2PO_4, 2.0 $CaCl_2$, 1.0 $MgCl_2$, and 25 glucose, equilibrated with 95% O_2/5% CO_2. Slices were incubated at 32°C for 30–45 min and then left at room temperature (20°C–22°C) until recordings were performed. All recordings were performed within 7 hr of slice cutting in a submerged slice chamber perfused with ACSF warmed to 32°C and equilibrated with 95% O_2/5% CO_2.

Electrophysiology

For all experiments other than those involving Ca uncaging (Figure 6), whole-cell recordings were made from CA1 pyramidal neurons visualized under infrared differential interference contrast (IR-DIC) on a combined two-photon imaging and uncaging microscope (Carter and Sabatini, 2004). Patch pipettes (open pipette resistance: 2.5–4.5 MΩ) were filled with an internal solution containing (in mM) 135 $KMeSO_4$, 10 HEPES, 4 $MgCl_2$, 4 NaATP, and 0.4 Na_2GTP, and 10 Na_2 Creatine Phosphate (pH 7.3). For the voltage-clamp experiments in Figure 2, $KMeSO_4$ was replaced with $CsMeSO_4$. For the experiments summarized in Figures 1, 2, and 3, 300 μM Fluo-5F (Molecular Probes, K_D ~1.1 μM) and 10 μM Alexa 594 (Molecular Probes) were included in the internal solution. In the voltage-step imaging experiments (Figure 4), the internal solution was based on that in Tai et al. (2006), and consisted of (in mM) 115 $CsMeSO_4$, 25 TEA-Cl, 10 HEPES, 4 Mg-ATP, and 0.5 Na-GTP (pH 7.2), with the addition of 20 μM Alexa 594 and 600 μM Fluo-5F. The Flou-5F concentration was increased for these experiments to minimize saturation of the indicator during the prolonged step depolarizations. For the UV Ca-uncaging experiments (Figure 6), CA1 pyramidal neurons were visualized with Dodt gradient contrast, and 1.25 mM $CaCl_2$, 0.6 mM $MgCl_2$, and 2 mM NP-EGTA (Invitrogen, Carlsbad, CA) were added to the K-based internal described above. Finally, for the electrical synaptic stimulation experiments in Figure 7, 50 μM EGTA was used in the K internal described above and Fluo-5 was omitted.

Recordings were made with an Axoclamp 200B amplifier (Axon Instruments, Union City, CA). Data were filtered at 5 kHz and sampled at 10 kHZ. Cells were held at −70 mV in voltage-clamp mode, and current was injected to hold cells at approximately −70 mV in current-clamp mode. Cells were rejected if holding currents exceed −100 pA. Series (not compensated) and input resistances were measured throughout the experiment, and recordings were discarded if series resistance exceeded 20 MΩ. In voltage-step experiments (Figures 4 and 5), capacitance and leakage currents were monitored and compensated for using a P/–4 protocol (Tai et al., 2006). D-serine (10 μM) was included in the ACSF to reduce NMDAR desensitization that can occur during glutamate uncaging. Liquid junction potentials of ~8 mV were not corrected.

Pharmacology

When appropriate and as listed in the text, pharmacological agents were used in the extracellular solution at the following final concentrations (in μM): 10 D-serine (Sigma-Aldrich, St. Louis, MO), 1 oxo-m (Tocris Biosciences, Ellisville, MO), 10 scopolamine hydrobromide (Tocris), 0.1 apamin (Calbiochem, La Jolla, CA), 20 CPP (Tocris), 10 NBQX (Tocris), 1 TTX (Tocris), 50 picrotoxin (Tocris), 3 nimodipine (Sigma-Aldrich), 1 ω-conotoxin-MVIIC (Peptides International, Louisville, KY), 0.3 SNX-482 (Peptides International), 10 mibefradil (Sigma-Aldrich), 0.1 Mtx-7 (Peptides International), 10 TBB (Sigma-Aldrich), 2000 CsCl (Sigma-Aldrich), 1000 4AP (Sigma-Aldrich), and 3000 $BaCl_2$ (Sigma-Aldrich). Experiments that used Mtx-7 and TBB included a 30 min incubation period in the recording chamber.

Combined 2PLSM and 2PLU

The experiments in Figures 1, 2, 3, 4, and 7 were performed using a custom built two-photon laser scanning microscope based on a BX51WI microscope (Olympus) as described previously (Carter and Sabatini, 2004). Two Ti-sapphire lasers (Mira/Verdi, Coherent) tuned to 840 and 725 nm were used for imaging and glutamate uncaging, respectively. In all uncaging experiments 3.75 mM MNI-glutamate (Tocris Cookson, Ellisville, MO) was included in a small volume (~9 ml) of recirculating ASCF. Uncaging laser pulse duration was 0.5 ms and power delivered to each spine was set to bleach ~30% of the red fluorescence in the spine head as described previously (Figure S1) (Bloodgood et al., 2009; Bloodgood and Sabatini, 2007). This corresponds to uncaging laser power at the back aperture of the objective of ~35 mW, similar to that used in other two-photon glutamate uncaging studies (Harvey et al., 2008). After laser power was set, the periphery of each spine was probed to identify the uncaging spot that triggered the largest somatic response, and uncaging at this spot was used for the remainder of the analysis (Busetto et al., 2008). This stimulation paradigm results in an average uEPSC of −14 pA (Figure 2) (Bloodgood and Sabatini, 2007) in voltage-clamped neurons in the presence of antagonists of voltage-gated channels. Such uEPSCs are similar to the larger-sized mEPSCs in these cells that are expected to arise from the higher-AMPAR-content, large spines studied here (Harris and Stevens, 1989; Matsuzaki et al., 2001). Image and electrophysiology acquisition was controlled by custom software written in MATLAB (Mathworks) and data analysis was performed using custom software written in Igor Pro (Wavemetrics).

Cells were filled with two fluorescent dyes: a Ca-insensitive fluorophore (Alexa Fluor 594), which fluoresces in the red (collected via 600–660 interference filter), and a Ca-sensitive fluorophore (Fluo-5F), which fluoresces in the green (collected via 500–550 interference filter). Red fluorescence was used to identify spines and dendrites. Relative differences in the amplitudes of intracellular Ca transients were judged by comparing the amplitude of green fluorescence transients as described previously (Bloodgood et al., 2009). Changes in fluorescence were quantified during the recording as: $\Delta G/R(t) = (F_{green}(t) - F_{rest,green})/(F_{red} - I_{dark,red})$. $F_{green}(t)$ is the green fluorescence signal as a function of time, $F_{rest,green}$ is the green fluorescence before stimulation, and $I_{dark,red}$ is the dark current in the red channel. G/R was separately measured in saturating Ca (G_{sat}/R) for each dye combination and batch of intracellular solution by imaging a sealed pipette filled with a mixture of equal volumes of intracellular solution and 1 M $CaCl_2$. ΔG/R measurements from the spine and dendrite were divided by G_{sat}/R, yielding the reported values of $\Delta G/G_{sat}$. This value is independent of the collection efficiencies of red and green photons and should be directly comparable across laboratories.

UV Uncaging of Intracellular Ca

For UV uncaging of Ca, we used a custom setup based on a BX51WI microscope (Olympus). The output of a 100 KHz pulsed q-switched UV laser (DPSS, Santa Clara, CA) producing ~1 W of 354.7 nm light was launched into a multimode, 200 μm inner diameter optical fiber with an numerical aperture of 0.22 (OZ Optics, Ottawa, Ontario, Canada). The beam was shuttered at the laser head (OZ Optics, part number HPUC-2,A3HP-355-M-10BQ-1-SH) and collimated at the output of the fiber (OZ Optics, part number HPUC0-2,A3HP-355-M-25BQ), resulting in a 10 mm diameter beam. This beam was focused on the back focal plane of a 60× water-immersion, infinity-corrected objective with a numerical aperture of 0.90 (Olympus) using a planoconvex lens. An iris was placed in the light path in a conjugate image plane to act as a field diaphragm. The iris was adjusted such that the diameter of the area in the tissue exposed to UV light was ~250 μm. Intensity was attenuated with a neutral density filter such that UV laser power measured at the back aperture of the objective was ~10 mW. Laser pulses were controlled by opening the shutter, waiting for mechanical vibrations in the fiber launch to dampen, and then q-switching the laser on and off.

Data Analysis and Statistics

The amplitudes of uncaging-evoked potentials and currents were measured as averages around their peak values with the exception of currents evoked at +40 mV, which were calculated by averaging 30–80 ms after the uncaging pulse to capture the NMDAR-mediated component of the current. The peaks of uncaging-evoked Ca transients were calculated by averaging 20–50 ms post uncaging. Amplitudes of Ca-activated K currents were calculated by averaging 150–200 ms after the end of the voltage step or 0–100 ms after the end of the UV uncaging pulse. These time windows were picked to isolate apamin-sensitive current (Figures 5 and 6). All data are expressed as the mean ± SEM. In the figures, average traces are shown as the mean (line) ± the SEM (shaded regions or bars). The decays of currents and fluorescence transients were analyzed by single exponential fits over monotonically decreasing regions of the traces in order to obtain a time constant of decay. A two-tailed t test was used to determine significance of differences in uEPSPs, uEPSCs, EPSPs, and $\Delta G/G_{sat}$ across conditions. For flow-in experiments, a paired t test was used on short averages from the baseline and the postwashin period. $p < 0.05$ was considered significant.

SUPPLEMENTAL INFORMATION

Supplemental Information includes two figures and one table and can be found with this article online at doi:10.1016/j.neuron.2010.09.004.

ACKNOWLEDGMENTS

We thank members of the Sabatini lab for helpful comments and critical reading of the manuscript. We also thank Bruce Bean and Wade Regehr for helpful discussions. This work was supported by grants (to B.L.S.) from the National Institute of Neurological Disorders and Stroke (NS046579) and (to A.J.G.) NIH (F31 NS065647) and Quan predoctoral fellowships.

Accepted: August 10, 2010
Published: December 8, 2010

REFERENCES

Allen, D., Fakler, B., Maylie, J., and Adelman, J.P. (2007). Organization and regulation of small conductance Ca2+-activated K+ channel multiprotein complexes. J. Neurosci. *27*, 2369–2376.

Andrásfalvy, B.K., Makara, J.K., Johnston, D., and Magee, J.C. (2008). Altered synaptic and non-synaptic properties of CA1 pyramidal neurons in Kv4.2 knockout mice. J. Physiol. *586*, 3881–3892.

Bildl, W., Strassmaier, T., Thurm, H., Andersen, J., Eble, S., Oliver, D., Knipper, M., Mann, M., Schulte, U., Adelman, J.P., and Fakler, B. (2004). Protein kinase CK2 is coassembled with small conductance Ca(2+)-activated K+ channels and regulates channel gating. Neuron *43*, 847–858.

Bloodgood, B.L., and Sabatini, B.L. (2007). Nonlinear regulation of unitary synaptic signals by CaV(2.3) voltage-sensitive calcium channels located in dendritic spines. Neuron *53*, 249–260.

Bloodgood, B.L., Giessel, A.J., and Sabatini, B.L. (2009). Biphasic synaptic Ca influx arising from compartmentalized electrical signals in dendritic spines. PLoS Biol. *7*, e1000190.

Borroni, A.M., Fichtenholtz, H., Woodside, B.L., and Teyler, T.J. (2000). Role of voltage-dependent calcium channel long-term potentiation (LTP) and NMDA LTP in spatial memory. J. Neurosci. *20*, 9272–9276.

Bourinet, E., Stotz, S.C., Spaetgens, R.L., Dayanithi, G., Lemos, J., Nargeot, J., and Zamponi, G.W. (2001). Interaction of SNX482 with domains III and IV inhibits activation gating of alpha(1E) (Ca(V)2.3) calcium channels. Biophys. J. *81*, 79–88.

Busetto, G., Higley, M.J., and Sabatini, B.L. (2008). Developmental presence and disappearance of postsynaptically silent synapses on dendritic spines of rat layer 2/3 pyramidal neurons. J. Physiol. *586*, 1519–1527.

Carter, A.G., and Sabatini, B.L. (2004). State-dependent calcium signaling in dendritic spines of striatal medium spiny neurons. Neuron *44*, 483–493.

Catterall, W.A. (2000). Structure and regulation of voltage-gated Ca2+ channels. Annu. Rev. Cell Dev. Biol. *16*, 521–555.

Catterall, W.A., Perez-Reyes, E., Snutch, T.P., and Striessnig, J. (2005). International Union of Pharmacology. XLVIII. Nomenclature and structure-function relationships of voltage-gated calcium channels. Pharmacol. Rev. *57*, 411–425.

Dawson, G.R., and Iversen, S.D. (1993). The effects of novel cholinesterase inhibitors and selective muscarinic receptor agonists in tests of reference and working memory. Behav. Brain Res. *57*, 143–153.

Deutsch, J.A. (1971). The cholinergic synapse and the site of memory. Science *174*, 788–794.

Drachman, D.A. (1977). Memory and cognitive function in man: does the cholinergic system have a specific role? Neurology *27*, 783–790.

Dutar, P., and Nicoll, R.A. (1988). Classification of muscarinic responses in hippocampus in terms of receptor subtypes and second-messenger systems: electrophysiological studies in vitro. J. Neurosci. *8*, 4214–4224.

Dutar, P., Bassant, M.H., Senut, M.C., and Lamour, Y. (1995). The septohippocampal pathway: structure and function of a central cholinergic system. Physiol. Rev. *75*, 393–427.

Ellis-Davies, G.C., and Kaplan, J.H. (1994). Nitrophenyl-EGTA, a photolabile chelator that selectively binds Ca2+ with high affinity and releases it rapidly upon photolysis. Proc. Natl. Acad. Sci. USA *91*, 187–191.

Everitt, B.J., and Robbins, T.W. (1997). Central cholinergic systems and cognition. Annu. Rev. Psychol. *48*, 649–684.

Faber, E.S.L., Delaney, A.J., and Sah, P. (2005). SK channels regulate excitatory synaptic transmission and plasticity in the lateral amygdala. Nat. Neurosci. *8*, 635–641.

Faber, E.S., Delaney, A.J., Power, J.M., Sedlak, P.L., Crane, J.W., and Sah, P. (2008). Modulation of SK channel trafficking by beta adrenoceptors enhances excitatory synaptic transmission and plasticity in the amygdala. J. Neurosci. *28*, 10803–10813.

Fernández de Sevilla, D., Núñez, A., Borde, M., Malinow, R., and Buño, W. (2008). Cholinergic-mediated IP3-receptor activation induces long-lasting synaptic enhancement in CA1 pyramidal neurons. J. Neurosci. *28*, 1469–1478.

Grunditz, A., Holbro, N., Tian, L., Zuo, Y., and Oertner, T.G. (2008). Spine neck plasticity controls postsynaptic calcium signals through electrical compartmentalization. J. Neurosci. *28*, 13457–13466.

Hammond, R.S., Bond, C.T., Strassmaier, T., Ngo-Anh, T.J., Adelman, J.P., Maylie, J., and Stackman, R.W. (2006). Small-conductance Ca2+-activated K+ channel type 2 (SK2) modulates hippocampal learning, memory, and synaptic plasticity. J. Neurosci. *26*, 1844–1853.

Harris, K.M., and Stevens, J.K. (1989). Dendritic spines of CA 1 pyramidal cells in the rat hippocampus: serial electron microscopy with reference to their biophysical characteristics. J. Neurosci. *9*, 2982–2997.

Harvey, C.D., and Svoboda, K. (2007). Locally dynamic synaptic learning rules in pyramidal neuron dendrites. Nature *450*, 1195–1200.

Harvey, C.D., Yasuda, R., Zhong, H., and Svoboda, K. (2008). The spread of Ras activity triggered by activation of a single dendritic spine. Science *321*, 136–140.

Keen, J.E., Khawaled, R., Farrens, D.L., Neelands, T., Rivard, A., Bond, C.T., Janowsky, A., Fakler, B., Adelman, J.P., and Maylie, J. (1999). Domains responsible for constitutive and Ca(2+)-dependent interactions between calmodulin and small conductance Ca(2+)-activated potassium channels. J. Neurosci. *19*, 8830–8838.

Kitajima, I., Yamamoto, T., Ohno, M., and Ueki, S. (1992). Working and reference memory in rats in the three-panel runway task following dorsal hippocampal lesions. Jpn. J. Pharmacol. *58*, 175–183.

Levey, A.I., Edmunds, S.M., Koliatsos, V., Wiley, R.G., and Heilman, C.J. (1995). Expression of m1-m4 muscarinic acetylcholine receptor proteins in rat hippocampus and regulation by cholinergic innervation. J. Neurosci. *15*, 4077–4092.

Lin, M.T., Luján, R., Watanabe, M., Adelman, J.P., and Maylie, J. (2008). SK2 channel plasticity contributes to LTP at Schaffer collateral-CA1 synapses. Nat. Neurosci. *11*, 170–177.

Madison, D.V., Lancaster, B., and Nicoll, R.A. (1987). Voltage clamp analysis of cholinergic action in the hippocampus. J. Neurosci. *7*, 733–741.

Magee, J.C. (1999). Dendritic Ih normalizes temporal summation in hippocampal CA1 neurons. Nat. Neurosci. *2*, 508–514.

Magee, J.C., and Cook, E.P. (2000). Somatic EPSP amplitude is independent of synapse location in hippocampal pyramidal neurons. Nat. Neurosci. *3*, 895–903.

Maingret, F., Coste, B., Hao, J., Giamarchi, A., Allen, D., Crest, M., Litchfield, D.W., Adelman, J.P., and Delmas, P. (2008). Neurotransmitter modulation of small-conductance Ca2+-activated K+ channels by regulation of Ca2+ gating. Neuron *59*, 439–449.

Marino, M.J., Rouse, S.T., Levey, A.I., Potter, L.T., and Conn, P.J. (1998). Activation of the genetically defined m1 muscarinic receptor potentiates N-methyl-D-aspartate (NMDA) receptor currents in hippocampal pyramidal cells. Proc. Natl. Acad. Sci. USA *95*, 11465–11470.

Markram, H., and Segal, M. (1990a). Acetylcholine potentiates responses to N-methyl-D-aspartate in the rat hippocampus. Neurosci. Lett. *113*, 62–65.

Markram, H., and Segal, M. (1990b). Long-lasting facilitation of excitatory postsynaptic potentials in the rat hippocampus by acetylcholine. J. Physiol. *427*, 381–393.

Martina, M., Turcotte, M.-E.B., Halman, S., and Bergeron, R. (2007). The sigma-1 receptor modulates NMDA receptor synaptic transmission and plasticity via SK channels in rat hippocampus. J. Physiol. *578*, 143–157.

Matsuzaki, M., Ellis-Davies, G.C., Nemoto, T., Miyashita, Y., Iino, M., and Kasai, H. (2001). Dendritic spine geometry is critical for AMPA receptor expression in hippocampal CA1 pyramidal neurons. Nat. Neurosci. *4*, 1086–1092.

Matsuzaki, M., Honkura, N., Ellis-Davies, G.C.R., and Kasai, H. (2004). Structural basis of long-term potentiation in single dendritic spines. Nature *429*, 761–766.

Mesulam, M. (2004). The cholinergic lesion of Alzheimer's disease: pivotal factor or side show? Learn. Mem. *11*, 43–49.

Millar, J.A., Barratt, L., Southan, A.P., Page, K.M., Fyffe, R.E., Robertson, B., and Mathie, A. (2000). A functional role for the two-pore domain potassium channel TASK-1 in cerebellar granule neurons. Proc. Natl. Acad. Sci. USA *97*, 3614–3618.

Ngo-Anh, T.J., Bloodgood, B.L., Lin, M., Sabatini, B.L., Maylie, J., and Adelman, J.P. (2005). SK channels and NMDA receptors form a Ca2+-mediated feedback loop in dendritic spines. Nat. Neurosci. *8*, 642–649.

Oertner, T.G., Sabatini, B.L., Nimchinsky, E.A., and Svoboda, K. (2002). Facilitation at single synapses probed with optical quantal analysis. Nat. Neurosci. *5*, 657–664.

Ramanathan, S., Tkatch, T., Atherton, J.F., Wilson, C.J., and Bevan, M.D. (2008). D2-like dopamine receptors modulate SKCa channel function in subthalamic nucleus neurons through inhibition of Cav2.2 channels. J. Neurophysiol. *99*, 442–459.

Randall, A.D., and Tsien, R.W. (1997). Contrasting biophysical and pharmacological properties of T-type and R-type calcium channels. Neuropharmacology *36*, 879–893.

Rouse, S.T., Marino, M.J., Potter, L.T., Conn, P.J., and Levey, A.I. (1999). Muscarinic receptor subtypes involved in hippocampal circuits. Life Sci. *64*, 501–509.

Rouse, S.T., Edmunds, S.M., Yi, H., Gilmor, M.L., and Levey, A.I. (2000). Localization of M(2) muscarinic acetylcholine receptor protein in cholinergic and non-cholinergic terminals in rat hippocampus. Neurosci. Lett. *284*, 182–186.

Sabatini, B.L., Oertner, T.G., and Svoboda, K. (2002). The life cycle of Ca(2+) ions in dendritic spines. Neuron *33*, 439–452.

Sah, P., and Isaacson, J.S. (1995). Channels underlying the slow afterhyperpolarization in hippocampal pyramidal neurons: neurotransmitters modulate the open probability. Neuron *15*, 435–441.

Schikorski, T., and Stevens, C.F. (1997). Quantitative ultrastructural analysis of hippocampal excitatory synapses. J. Neurosci. *17*, 5858–5867.

Schneggenburger, R., and Neher, E. (2000). Intracellular calcium dependence of transmitter release rates at a fast central synapse. Nature *406*, 889–893.

Shinoe, T., Matsui, M., Taketo, M.M., and Manabe, T. (2005). Modulation of synaptic plasticity by physiological activation of M1 muscarinic acetylcholine receptors in the mouse hippocampus. J. Neurosci. *25*, 11194–11200.

Stackman, R.W., Hammond, R.S., Linardatos, E., Gerlach, A., Maylie, J., Adelman, J.P., and Tzounopoulos, T. (2002). Small conductance Ca2+-activated K+ channels modulate synaptic plasticity and memory encoding. J. Neurosci. *22*, 10163–10171.

Steiner, P., Higley, M.J., Xu, W., Czervionke, B.L., Malenka, R.C., and Sabatini, B.L. (2008). Destabilization of the postsynaptic density by PSD-95 serine 73 phosphorylation inhibits spine growth and synaptic plasticity. Neuron *60*, 788–802.

Tai, C., Kuzmiski, J.B., and MacVicar, B.A. (2006). Muscarinic enhancement of R-type calcium currents in hippocampal CA1 pyramidal neurons. J. Neurosci. *26*, 6249–6258.

Taverna, S., Tkatch, T., Metz, A.E., and Martina, M. (2005). Differential expression of TASK channels between horizontal interneurons and pyramidal cells of rat hippocampus. J. Neurosci. *25*, 9162–9170.

Woolf, N.J. (1991). Cholinergic systems in mammalian brain and spinal cord. Prog. Neurobiol. *37*, 475–524.

Xia, X.M., Fakler, B., Rivard, A., Wayman, G., Johnson-Pais, T., Keen, J.E., Ishii, T., Hirschberg, B., Bond, C.T., Lutsenko, S., et al. (1998). Mechanism of calcium gating in small-conductance calcium-activated potassium channels. Nature *395*, 503–507.